

Investigation of $\text{La}_{0.8}\text{Sr}_{0.2}\text{CoO}_3/\text{Ce}_{0.85}\text{Sm}_{0.15}\text{O}_{2-x}$ cathode performance of solid oxide fuel cell by electrochemical impedance spectroscopy: Effect of firing temperature

Mali Hunsom[†], Liliya A. Dunyushkina and Stuart B. Adler*

Department of Chemical Technology, Faculty of Science, Chulalongkorn University, Phaya Thai, Bangkok, 10330, Thailand

*Department of Chemical Engineering, University of Washington, Box 351750, Seattle, WA 98195, USA

(Received 29 December 2005 • accepted 9 March 2006)

Abstract—Perovskite type complex oxide $\text{L}_{0.8}\text{Sr}_{0.2}\text{CoO}_{3-\delta}$ symmetrical cells were prepared on Samaria doped ceria electrolyte $\text{Ce}_{0.85}\text{Sm}_{0.15}\text{O}_{2-x}$ by using the screen-printing method in a laboratory scale. The performance of the symmetrical cell was investigated by using electrochemical spectroscopy at frequency ranging from 0.1-300 kHz. Effect of firing temperature from 975-1,050 °C was investigated under the controlled oxygen pressure from 0.002-0.21 atm and controlled measuring temperature from 635-782 °C. The preliminary results indicated that, for all cells prepared at different firing temperatures, the SEM and XRD did not indicate any differences between them. By using EIS, however, two impedance arcs were obviously observed. This first arc was found at high frequency region ($>1,000$ Hz) and the second one was observed at low frequency region (<10 Hz). The high frequency arc corresponded to the impedance of electron-transfer and ion-transfer processes occurring at the current collector/electrode and electrode/electrolyte interfaces. The low frequency arc was the convoluted contribution of the diffusion processes (non-charge transfer processes). Changing firing temperature, measuring temperature and oxygen pressure leads to changing of symmetrical cell performances. The activation energy of these symmetrical cells was around 1.5-2.0 eV depending on the firing temperature and oxygen pressure.

Key words: Symmetrical Cell, A.C. Impedance, Firing Temperature, Perovskite, Solid Oxide Fuel Cell

INTRODUCTION

Among various kinds of power generators, solid oxide fuel cells (SOFCs) are believed to become high efficiency power generators in the next century due largely to environmental friendly, fuel-versatile electric power. SOFCs are operated at high temperature, so they offer several potential advantages including reversible electrode reactions, low internal resistance, high tolerance to typical catalyst poison, possibility of burning other fuels besides H_2 , CH_4 and the production of high-quality waste heat for reformation of liquid fuels [Adler, 2004]. For example, by using CH_4 as a gaseous fuel, the generated electricity of the SOFC with 1 wt% $\text{Sr/La}_2\text{O}_3\text{-BiO}_3\text{-Ag-YSZ}$ membrane increased by decreasing in C_2 selectivity and increasing in CH_4 conversion [Guo et al., 1998]. In addition, this type of fuel cell is much closer to commercial reality due to technological advances in electrode composition, microstructure control, thin-film ceramic fabrication, and stack & system design. In SOFC, a negative charge ion (O^{2-}) is transferred from the cathode through the electrolyte to the anode and thus the product water is formed at the anode. The recently state-of-the-art electrolyte is zirconia based electrolyte. Above a temperature of 800 °C, zirconia becomes a conductor of oxygen ions (O^{2-}), which presents both challenges for construction and durability, and also opportunities in combined cycle applications in the range of 800-1,000 °C. The anode material is usually a mixture of ceramic and metal known as zirconia cermets. A popular metal component is nickel because of its high electronic conductivity and its stability under chemically reducing and partial

reducing conditions [Larminie and Dicks, 2003]. Strontium doped lanthanum manganite, a *p*-type semiconductor, is the most commonly used as a cathode material due to its porous structure that must allow fast mass transport of reactant and product gas. Other attractive material for cathode side is the *p*-type conducting called perovskite structure. This type of catalyst has been applied for decomposition of nitric oxide [Klvanova et al., 1999], for hydrocarbon oxidation [Klvanova et al., 2002], for natural gas combustion [Rosso et al., 2003] and for oxygen reduction in high temperature fuel cells such as SOFC. The composite $\text{L}_{1-x}\text{Sr}_x\text{MnO}_{3-\delta}/\text{YSZ}$ (LSM/YSZ) electrodes exhibit high electrochemical performance and are appropriate for being a cathode material for SOFC due to its broad electrochemical reaction site and its electrochemical characteristics [Jorgensen et al., 1999; Lee, 2002]. The chemical stability of the conventional LSM can be improved by applying an interlayer of electrolyte, $(\text{Y}_2\text{O}_3)_{0.15}(\text{CeO}_2)_{0.85}$ and $\text{Ce}_{0.8}\text{Gd}_{0.2}\text{O}_{1.9}$ between YSZ and cathode [Charojrochukul et al., 1999]. For intermediate temperature SOFC (550-750 °C), the $\text{Ln}_{1-x}\text{Sr}_x\text{Co}_{1-x}\text{Fe}_y\text{O}_{3-\delta}$ (LSCF) compositions showed high ionic and electronic conductivity as well as high catalytic activity for oxygen reduction [Adler, 1998]. Doping of Pt, Pd and Ag to the LSCF catalyst can promote catalyst activity [Sahibzada et al., 1998; Wang et al., 2002]. The material $\text{Dy}_{0.6}\text{Sr}_{0.4}\text{Co}_{0.2}\text{Fe}_{0.8}\text{O}_{3-\delta}$ (Dy-SCF) showed higher catalytic activity for oxygen dissociation at this temperature range [Gao, 2003]. Besides LSCF catalyst, Co-containing perovskites $\text{La}_{1-x}\text{Sr}_x\text{Mn}_{1-y}\text{Co}_y\text{O}_3$ (LSMC) showed good chemical compatibility with ceria-based electrolytes [Chen, 2003]. To reduce the cost of SOFC, the development of low temperature SOFC becomes necessary. The performance of SOFC, however, is strongly influenced by the electrochemical properties of the cathode. A candidate cathode material for low temperature SOFC is $\text{La}_{1-x}\text{Sr}_x\text{CoO}_3$ (LSCO).

[†]To whom correspondence should be addressed.

E-mail: mali.h@chula.ac.th

It is a perovskite-type complex oxide with a very high electronic conductivity [Petrov et al., 1995] and high oxide ionic conductivity [Sekido et al., 1990]. Preparation of LSCO electrode on YSZ electrolyte produced an intermediate phase due to the diffusion of LSCO into YSZ. This can be minimized by depositing a thin layer of ceria electrolyte [Charojrochkul et al., 1999]. By using the pulsed laser deposition technique, the LSCO epitaxial films grew with a (110) preferred orientation on YSZ (100), while the porous polycrystalline films were formed on YSZ by the annealing of LSCO samples deposited at low temperature [Chen et al., 1999; Yuemei et al., 2001]. Symmetrical cell of LSCO/ceria/LSCO was fabricated and measured at various conditions [Adler, 2000]. The measurement indicated that O_2 was reduced chemically at the porous mixed conductor surface, and followed by diffusion of oxygen through the mixed conductor to the electrolyte.

In the present study, we attempted to investigate the effect of the firing temperature in a small temperature range ($<75^\circ\text{C}$) of the perovskite type complex oxide from symmetrical LSCO/ceria/LSCO and tested under the controlled oxygen pressures and temperatures.

EXPERIMENTAL

The electrolyte, Samaria doped ceria $\text{Ce}_{0.8}\text{Sm}_{0.2}\text{O}_{2-x}$, was cut as a square piece having a dimension of 2.54×2.54 cm and fired in the furnace (Deltech DT-31-THM-666-Y550-00) at a controlled temperature. Then LSCO 82 ink ($\text{La}_{0.8}\text{Sr}_{0.2}\text{CoO}_3$) with composition of $x=0.2$ was printed on the first surface of electrolyte by screen-printing method (Ami MSP-053) and consequently fired in the furnace (Paragon DTC 800C). After that, the other surface was done by the similar procedure. Three firing temperatures were used including 975°C , $1,000^\circ\text{C}$, and $1,050^\circ\text{C}$. The active surface area of each side of the catalyst was around 1 cm^2 . The quality of printed film and surface morphology of the prepared catalysts were tested by using the XRD (Philips PW 1830 generator) and SEM (JEOL JSM 5200), respectively.

The AC-impedance spectroscopy method was used to investigate the reduction reaction of oxygen on the prepared catalyst under the controlled atmosphere and temperature. The potentiostat (Solartron SI 1287 and EG&G PARC 362) and the frequency response analyzer (Solartron 1252A) connected with the computer were used to analyze the performance of the electrode. Impedance data were recorded in the frequency ranging from 0.1-300 kHz with applied AC amplitudes 20 mV. The performance of symmetrical cells was mea-

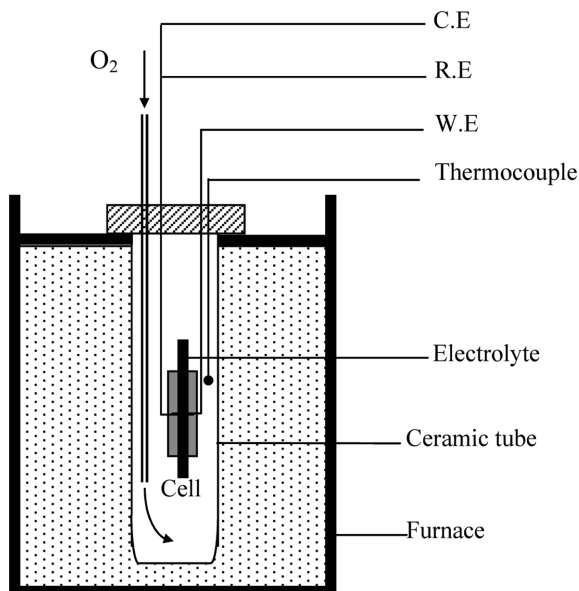


Fig. 1. Schematic diagram of AC-impedance apparatus.

ured between 635 and 782°C under various oxygen pressures ($p\text{O}_2$); 0.002 atm O_2/N_2 , 0.01 atm O_2/N_2 , and 0.21 O_2/N_2 . Fig. 1 shows the configuration of the apparatus used to measure the cell impedance.

RESULTS AND DISCUSSION

The surface morphology and cross-section of LSCO/ceria/LSCO catalysts prepared at various firing temperatures are shown in Fig. 2 and 3. For all firing temperatures, the SEM indicated that all catalysts show porous structures. Large pores of $1.5\text{-}2\text{ }\mu\text{m}$ occur and are surrounded by smaller pores of $0.2\text{-}0.8\text{ }\mu\text{m}$. The average porosity of all catalyst is around 41% at the same magnification. The film thicknesses of the porous LSCO layer are around 4 , 5 , and $6\text{ }\mu\text{m}$ at firing temperature of 975°C , $1,000^\circ\text{C}$ and $1,050^\circ\text{C}$, respectively.

Fig. 4 shows the X-ray pattern of the LSCO catalyst prepared at various firing temperatures. For all firing temperatures, ceria peaks form a very strong background and cover a few LSCO peaks. The peaks of catalysts prepared at $1,000^\circ\text{C}$ and $1,050^\circ\text{C}$ occur at the same two-theta position and they have a little bit higher than that of the catalyst prepared at 975°C . A small peak of an unidentified impurity is observed at low sintering temperature, 975°C , at $2\theta=$

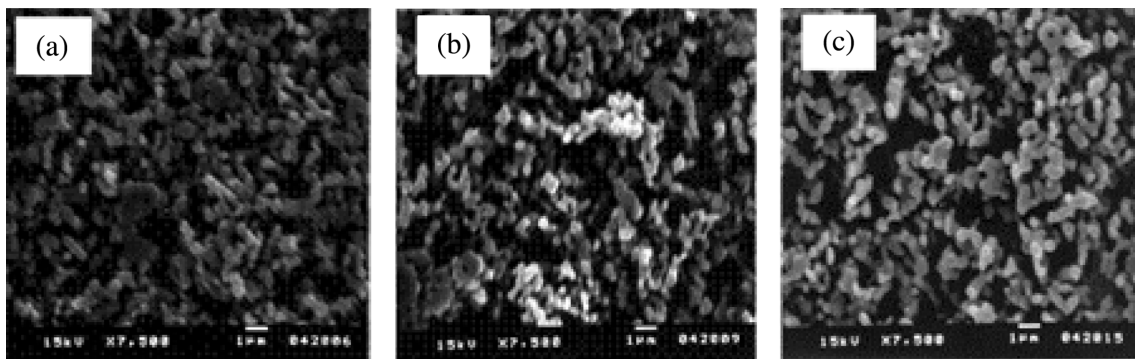


Fig. 2. Surface morphology of LSCO catalyst prepared at (a) 975°C , (b) $1,000^\circ\text{C}$, and (c) $1,050^\circ\text{C}$ at $7,500\times$ magnification.

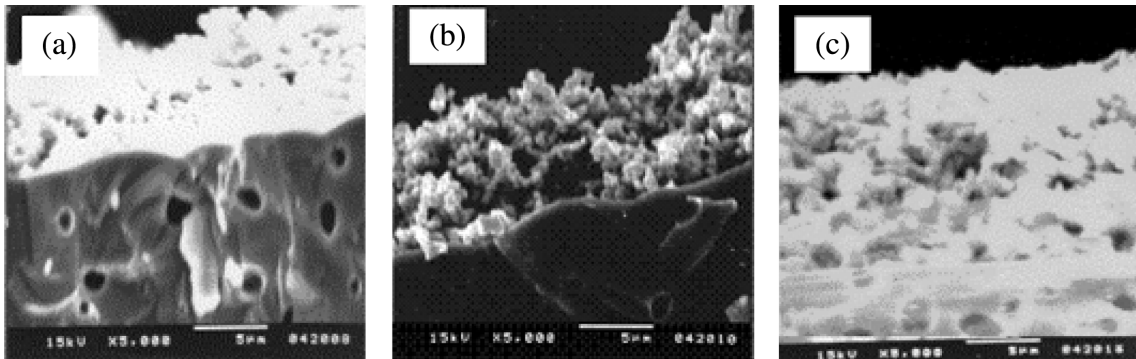


Fig. 3. A cross-section of LSCO/ceria/LSCO prepared at (a) 975 °C, (b) 1,000 °C, and (c) 1,050 °C at 5,000× magnification.

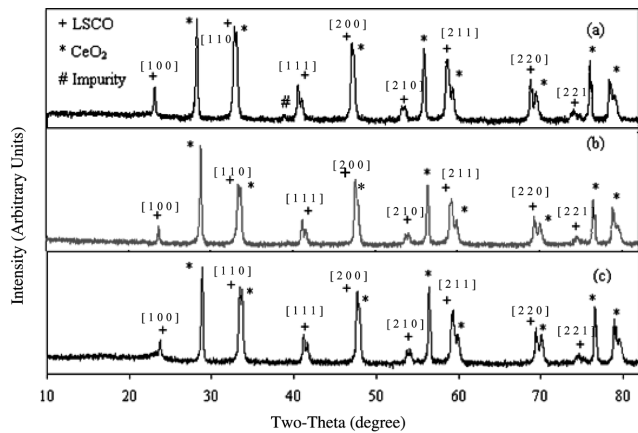


Fig. 4. X-ray diffraction pattern of LSCO/ceria/LSCO at (a) 975 °C, (b) 1,000 °C, and (c) 1,050 °C.

According to the results of this part, both XRD patterns and SEM do not indicate any differences after firing at different temperatures.

Impedance spectroscopy was used to determine the performance of symmetrical LSCO/ceria/LSCO cells at various temperatures and oxygen pressures. Fig. 5 shows the impedance plot of this electrode prepared at different firing temperatures. The spectra reveal the presence of an inductance, on the order of 2 μ H, at frequencies above 47 kHz. For each firing temperature, two impedance arcs at low frequencies are obviously observed similar to the previous works of the perovskite catalysts [Lane et al., 1995; Anderson et al., 1995]. The high frequency arc reaches the maximum imaginary part at around 1,500 Hz, whereas the low frequency arc reaches the maximum imaginary part at around 6 Hz. At the lower firing temperature, the high frequency arc is bigger than that at the higher firing temperature and it decreases when the firing temperature increases. Based on the ALS model of this catalyst [Adler et al., 1997], it can be suggested that the high frequency arc may correspond to the charge transfer processes consisting of electronic transfer and ionic transfer processes at the current collector/electrode and electrode/electrolyte interface, while the low frequency arc is the contribution of non-charge-transfer processes. Higher firing temperature can reduce the interface impedance because it changes the microstructure and conductivity of the catalysts [Charojrochukul et al., 1999]. At frequency below 0.6 Hz, a deviation of spectra is observed for all electrodes especially for the lower measuring temperature. The cause of these deviations is not investigated here due to the complication of data interpretation.

The total activation energy of the electrode is calculated as a function of reciprocal absolute firing temperature at various oxygen pressures, 0.002, 0.01 and 0.21 atm, as shown in Fig. 6. The activation energy increases slightly as the firing temperature decreases because a high firing temperature can promote the crystalline structure of the symmetrical cell. In air ($p_{O_2}=0.21$ atm), it was found to be 1.76, 1.75, and 1.52 eV at 975, 1,000, and 1,050 °C, respectively. These results are almost close to the results of the previous works of this perovskite type [Yamamoto et al., 1987]. Increasing oxygen pressure leads to decreasing electrode activation energy.

Effect of measuring temperature was investigated at temperature ranging from 635 °C to 782 °C under controlled oxygen pressures as shown in Fig. 7. The electrode resistance for both low and high frequency arcs decreases with the increase of measuring temperature. In addition, the increase of the measuring temperature leads to the decrease of the electrolyte resistance because high operating

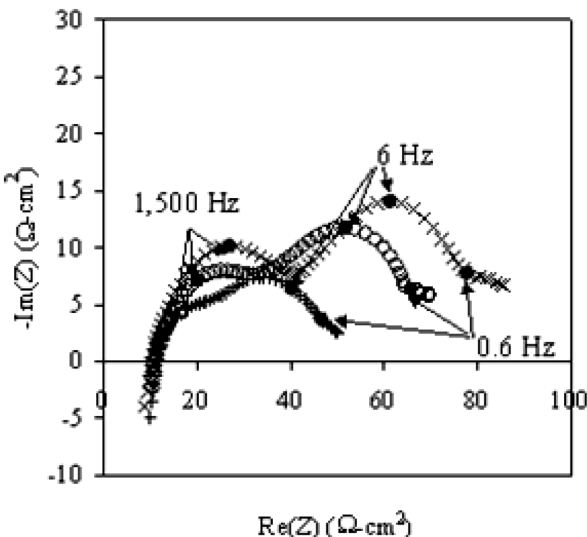


Fig. 5. Example of Nyquist plot of symmetrical LSCO/ceria/LSCO cell at different firing temperatures and $p_{O_2}=0.21$. $T_f=975$ °C (x); $T_f=1,000$ °C (○); $T_f=1,050$ °C (+).

38.87 degree, which disappears when the catalyst was prepared at high temperature. Nevertheless, the lattice structures of the prepared LSCO catalysts are similar, namely, they are present in the rhombohedral structure with the rhombohedral angle (α) close to 90.5°.

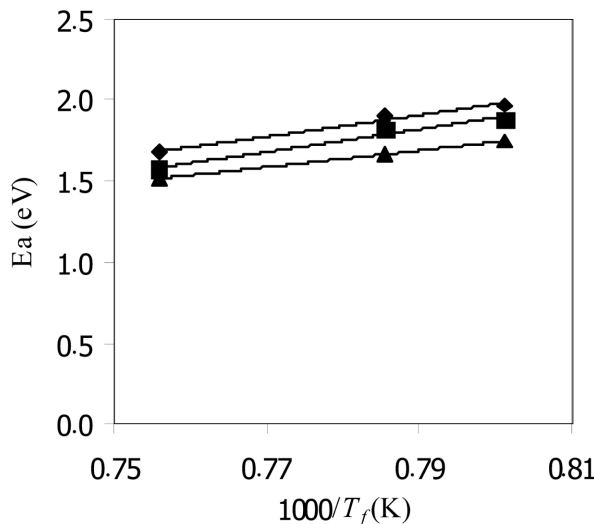


Fig. 6. Activation energy of symmetrical LSCO/ceria/LSCO electrode at different firing temperatures. $p\text{O}_2=0.21$ atm (◆); $p\text{O}_2=0.01$ atm (■); $p\text{O}_2=0.002$ atm (▲).

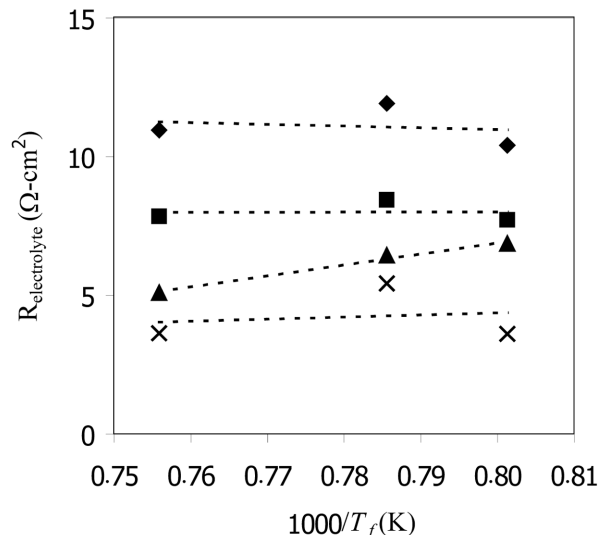


Fig. 8. Plot of electrolyte resistance as a function of firing temperature at $p\text{O}_2=0.21$. $T_m=635$ °C (◆); $T_m=685$ °C (■); $T_m=742$ °C (△); $T_m=782$ °C (×).

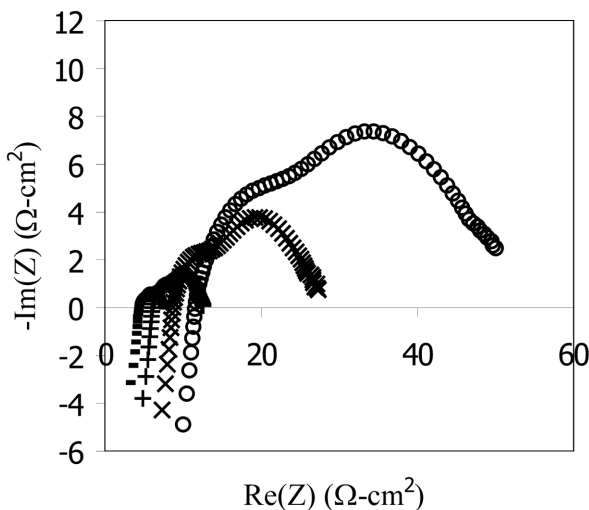


Fig. 7. Impedance plot of LSCO/ceria/LSCO at different measuring temperatures at $p\text{O}_2=0.21$. $T_m=635$ °C (○); $T_m=685$ °C (×); $T_m=742$ °C (+); $T_m=782$ °C (−); $T_m=782$ °C (○).

temperature can promote an ionic and electronic conductivity of the electrolyte and cathode materials. Fig. 8 shows the plot of electrolyte resistance as a function of firing temperatures at various measuring temperatures in the air. The difference of firing temperatures has a small effect on electrolyte resistance measured at the same condition. Those are 11.10 ± 0.71 $\Omega\text{-cm}^2$, 8.00 ± 0.38 $\Omega\text{-cm}^2$, 6.13 ± 0.92 $\Omega\text{-cm}^2$, and 4.23 ± 1.05 $\Omega\text{-cm}^2$ at 635 °C, 685 °C, 742 °C, 782 °C measuring temperatures, respectively.

Effect of oxygen pressure was investigated at several values (0.002, 0.01, and 0.21 atm). Two arcs are still observed for each oxygen pressure as shown in Fig. 9. Changing oxygen pressure has a strong effect on the low frequency arc spectra, whereas it has no effect on the high frequency spectra. At 0.002 atm, the low frequency arc spectra are bigger than that at high frequency arc. For higher oxygen pressure, however, the high frequency arc spectra become smaller.

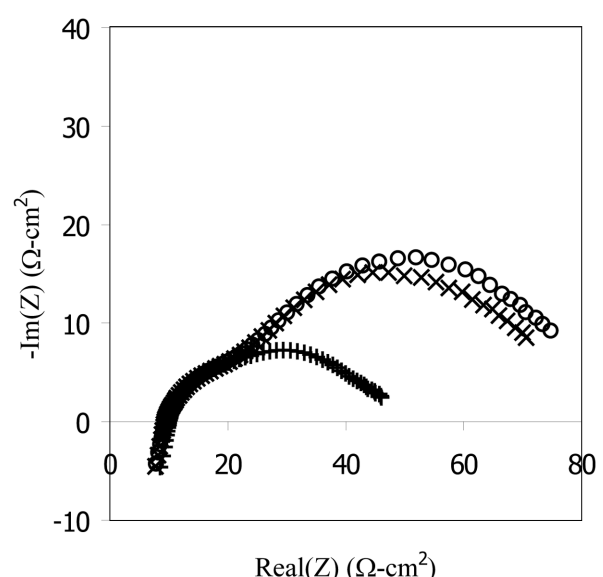


Fig. 9. Impedance plot of LSCO/ceria/LSCO at different measuring pressure at $T_m=635$ °C. $p\text{O}_2=0.21$ atm (+); $p\text{O}_2=0.01$ atm (×); $p\text{O}_2=0.002$ atm (○).

This is because high oxygen pressure can reduce the diffusion processes of oxygen in the system. The relationships between the capacitance and the firing temperature and measuring temperature are shown in Fig. 10.

Two values of the capacitance were separately calculated. For both arcs, the capacitance increases as a function of measuring temperature. For the higher firing temperature, however, the capacitance at the high frequency arc increases, whereas that at the low frequency arc remains constant. For all measuring temperatures, the capacitances at the high and low frequency arcs are about 0.01-0.1, and 0.1-10 mF/cm², respectively. From previous work, it is suggested that the value of double layer capacitance (C_{dl}) indicates the

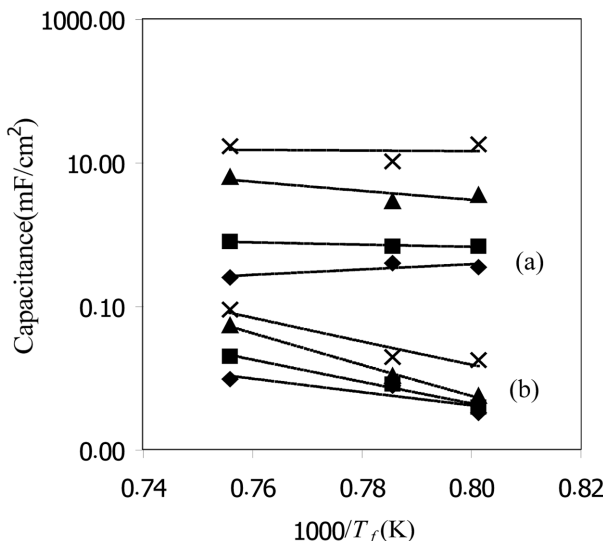


Fig. 10. Plot of capacitance at different firing temperature: (a) low frequency capacitance; (b) high frequency capacitance. $T_f = 635\text{ }^\circ\text{C}$ (\blacklozenge); $T_f = 685\text{ }^\circ\text{C}$ (\blacksquare); $T_f = 742\text{ }^\circ\text{C}$ (σ); $T_f = 782\text{ }^\circ\text{C}$ (\times).

surface area of the three-phase boundary [Sasaki et al., 1991]. The larger the C_{dl} value, the larger the surface area of the three-phase boundary.

CONCLUSIONS

LSCO 82 symmetrical cells were prepared on ceria electrolyte by using the screen-printing method and their performance was tested by using electrochemical impedance spectroscopy. Effect of firing temperature was investigated under the controlled pressures and controlled temperatures. For all firing temperatures, two impedance arcs are obviously observed. This first one occurs at the high frequency region ($>1,000\text{ Hz}$), which may correspond to the electronic and ionic transports. The last one is observed at the low frequency region ($<10\text{ Hz}$), which corresponds to the oxygen diffusion process. The firing temperature has a strong effect on the total electrode resistance but a small effect on the electrolyte resistance. On the other hand, the measuring temperature has a strong effect on both electrode and electrolyte resistances. Changing the oxygen pressure has a large influence on the impedance spectra at the low frequency region, whereas it has a small effect on that at the high frequency region. Increasing the oxygen pressure leads to a size reduction of the spectra at the low frequency arc. The total activation energy of the symmetrical cell changes as an inverse function of firing temperatures and oxygen pressures. It decreases when firing temperature and oxygen pressure increase.

ACKNOWLEDGMENTS

The authors would like to thank the ADB under The Petroleum and Petrochemical Technology Consortium, Chulalongkorn University for financial support of our project.

REFERENCES

Adler, S. B., "Mechanism and kinetics of oxygen reduction on porous $\text{La}_{1-x}\text{Sr}_x\text{CoO}_{3-\delta}$ electrodes," *Solid State Ionics*, **111**, 125 (1998).

Adler, S. B., "Limitations of charge-transfer models for mixed-conducting oxygen electrodes," *Solid State Ionics*, **135**, 603 (2000).

Adler, S. B., *Factor governing oxygen reduction in solid oxide fuel cell cathodes-A review*, Department of chemical Engineering, University of Washington (2004).

Adler, S. B., Lane, J. A. and Steele, B. C. H., "Electrode kinetics of porous mixed-conducting oxygen electrodes," *J. Electrochem. Soc.*, **144**, 1884 (1997).

Anderson, H. U., Tai, L. W., Chen, C. C., Nasrallah, M. M. and Huebner, W.; in Doliya, M., Yamamoto, O., Tagawa, H. and Singhal, S. C., (Eds.), *Solid oxide fuel cells IV*, PV 95-1, 375, The Electrochemical Society Proceeding Series, Pennington, NJ (1995).

Charojrachkul, S., Choy, K. L. and Steele, B. C. H., "Cathode/electrolyte system for solid oxide fuel cells fabricated using flame assisted vapor deposition technique," *Solid State Ionics*, **21**, 107 (1999).

Chen, X., Wu, N. J., Ritums, D. L. and Gnatiev, A. I., "Pulsed laser deposition of conducting porous La-Sr-Co-O films," *Thin Solid Films*, **342**, 61 (1999).

Chen, W., Wen, T., Nie, H. and Zheng, R., "Study of $\text{Ln}_{0.6}\text{Sr}_{0.4}\text{Co}_{0.8}\text{Mn}_{0.2}\text{O}_{3-\delta}$ ($\text{Ln}=\text{La, Gd, Sm or Nd}$) as the cathode materials for intermediate temperature SOFC," *Mat. Res. Bull.*, **38**, 1319 (2003).

Gao, J., Liu, X., Peng, D. and Meng, G., "Electrochemical behavior of $\text{Ln}_{0.6}\text{Sr}_{0.4}\text{Co}_{0.2}\text{Fe}_{0.8}\text{O}_{3-\delta}$ ($\text{Ln}=\text{Ce, Gd, Sm, Dy}$) materials used as cathode of IT-SOFC," *Catal. Today*, **82**, 207 (2003).

Guo, X. M., Hidajat, K. and Chaing, C. H., "An experimental study of oxidative coupling of methane in a solid oxide fuel cell with 1 wt% $\text{Sr/La}_2\text{O}_3\text{-BiO}_3\text{-Ag-YSZ}$ membrane," *Korean J. Chem. Eng.*, **15**, 469 (1998).

Jorgensen, M. J., Primdahl, P. and Mogensen, M., "Characterization of composite SOFC cathodes using electrochemical impedance spectroscopy," *Electrochimica Acta*, **44**, 4195 (1999).

Klavana, D., Kirchnerova, J. and Tofan, C., "Catalytic decomposition of nitric oxide by perovskites," *Korean J. Chem. Eng.*, **16**, 470 (1999).

Klavana, D., Song, K. S. and Kirchnerova, J., "Catalytic performance of $\text{La}_{0.66}\text{Sr}_{0.34}\text{Co}_{0.2}\text{Fe}_{0.8}\text{O}_3$ perovskite in propane combustion: effect of preparation and specific surface area," *Korean J. Chem. Eng.*, **19**(6), 932 (2002).

Lane, J. A., Adler, S., Middleton, P. H. and Steele, B. C. H.; in Doliya, M., Yamamoto, O., Tagawa, H. and Singhal, S. C. (Eds.), *Proceedings of the Fourth International Symposium on Solid Oxide Fuel Cells*, The Electrochemical Soc., New Jersey (1995).

Larminie, J. and Dicks, A., *Fuel cell systems explained*, John Wiley & Sons (2003).

Lee, H. K., "Electrochemical characteristics of $\text{La}_{1-x}\text{Sr}_x\text{MnO}_3$ for solid oxide fuel cell," *Mat. Chem. Phys.*, **77**, 639 (2002).

Petrov, A. N., Kononchuk, O. F., Andreev, A. V., Cherepanov, V. A. and Kofstad, P., "Crystal structure, electrical and magnetic properties of $\text{La}_{1-x}\text{Sr}_x\text{CoO}_{3-\delta}$," *Solid State Ionics*, **80**, 189 (1995).

Rosso, I., Saracco, G. and Specchia, V., "Tackling the problem of sulfur poisoning of perovskite catalysts for natural gas combustion," *Korean J. Chem. Eng.*, **20**, 222 (2003).

Sahibzada, M., Benson, S. J., Rudkin, R. A. and Kilner, J. A., "Pd-promoted $\text{La}_{0.6}\text{Sr}_{0.4}\text{Co}_{0.2}\text{Fe}_{0.8}\text{O}_3$ cathodes," *Solid State Ionics*, **113-115**, 285 (1998).

Sekido, S., Tachibana, H., Yamamura, Y. and Kambara, T., "Electric-

ionic conductivity in perovskite-type oxides, $\text{Sr}_x\text{La}_{1-x}\text{Co}_{1-y}\text{Fe}_y\text{O}_{3-\delta}$,” *Solid State Ionics*, **37**, 253 (1990).

Sasaki, J., Mizusaki, J. and Yamauchi, S., “Studies on electrode processes of stabilized zirconia cells by the complex impedance method,” *Solid State Ionics*, **3-4**, 531 (1984).

Wang, S., Kato, T., Nagata, S., Honda, T., Kaneko, T., Iwashita, N. and Dokiya, M., “Performance of a $\text{La}_{0.6}\text{Sr}_{0.4}\text{Co}_{0.8}\text{Fe}_{0.2}\text{O}_3\text{-Ce}_{0.8}\text{Gd}_{0.2}\text{O}_{1.9}$ -Ag cathode for ceria electrolyte SOFCs,” *Solid State Ionics*, **146**, 203 (2002).

Yuemei, L. Y., Jacobson, A. J., Chen, C. L., Luo, G P., Ross, K. D. and Chu, C. W., “Oxygen exchange kinetics on a highly oriented $\text{La}_{0.5}\text{Sr}_{0.5}\text{CoO}_{3-\delta}$ thin film prepared by pulsed-laser deposition,” *Appl. Phys. Lett.*, **79**, 776 (2001).

Yamamoto, O., Takeda, Y., Kanno, R. and Noda, M., “Perovskite-type oxides as oxygen electrodes for high temperature oxide fuel cells,” *Solid State Ionics*, **22**, 241 (1987).